Brodogradnja/Shipbuilding/Open access Volume 74 Number 2, 2023

Dario Ban

http://dx.doi.org/10.21278/brod74201

ISSN 0007-215X
eISSN 1845-5859

Re-examination of centre of buoyancy curve and its evolute for rectangular cross section, Part 1: Swallowtail discontinuity bounds

UDC 629.5.015.11:629.5.012.65:629.5.024.5
Original scientific paper

Summary

At the beginning of the naval architecture theory, in the 18th century, Bouguer and Euler set the foundations of naval architecture with the centre of buoyancy and metacentric curve definition. After that, in 20th century, it is determined from bifurcation and catastrophe theory developed by Thom, and its application for ships in works of Zeeman, Stewart and others, that the centre of buoyancy curve for the rectangular cross section consists of parabola and hyperbola equations, but no exact equations are given for the hyperbola segment of that curve. Therefore, the hyperbola segment of the centre of the buoyancy curve is re-examined in this paper with emphasis on belonging metacentric locus curve as the evolute of the centre of the buoyancy curve. The observed metacentric curve consists of semi-cubic parabolas and Lamé curves with 2/3 exponent and negative sign, resulting in the cusp discontinuities in the symmetry of functions definition. Belonging swallowtail discontinuity in the hyperbola range between two heel angles of the rectangular cross section deck immersion/bottom emersion angles is examined, depending on existence of extremes of belonging hyperbola curve. After that, the single condition for hyperbola extreme the existence is given with the belonging new lower and upper non-dimensional bounds of rectangle cross section dimensions.

Keywords: *metacentric curve; rectangular cross section; cuspidal Lamé curve, cusp discontinuity; swallowtail; bounds*

1 Introduction

1.1 Basic theory about metacentric locus curve

One of the most important hydrostatic properties for the determination of a ship's equilibrium is the centre of the buoyancy locus curve, i.e. the centre of buoyancy evolute or metacentric M-curve, representing the distances between the ship's coordinate system origin K and the actual metacentre M position for different longitudinal and transversal inclination angles. Its characteristics were examined by many naval architecture researchers from the beginning of the naval architecture theory development with a focus on initial stability characteristics (Bouguer, [1], Euler, [2]), while today whole metacentric curve characteristics are examined using modern bifurcation/catastrophe/singularity theory (Thom, [3], Zeeman,

[4], Poston and Stewart, [5], Arnold, [6]) and as a part of singularity theory or control theory, by many other papers and researches like in Senjanović & Fan Yin, [7], [8], Neves et al., [9], [10], Makai et al., [11], and Zhang et al., [12]. Recently, in naval architecture theory, various works are done on theoretical and practical aspects of the ship's equilibrium and stability by Spyrou, [13], Nowacki, [14], Francescutto & Papanikolau, [15], Francescutto, [16], Megel et al., [17], Hantoro et al., [18], Karolius et al., [19], Santos et al., [20], and others, with metacentric locus and metacentric height as one of the main variables in stability evaluation, in general.

In this paper, the existence of swallowtail discontinuity of metacentric locus curve for rectangular cross section, defined in the works of Zeeman, [4], and Poston & Stewart, [5], is re-examined, to set new bounds for its occurrence based on non-dimensional ratios of rectangle's floatation properties. For rectangular cross section with breadth B, height D and draught d, the centre of buoyancy B-curve consists of eight quadratic function segments in general, four parabolas and four hyperbolas as shown in Fig. 1 below, depending on ratios $\lambda = d/D$ and $w = B/(2D)$, and immersed rectangle diagonal angle β, as set in [4] and [5] with definitions:

Definition 1: Centre of buoyancy B-curve properties for rectangular cross section

The centre of buoyancy B-curve for rectangular cross section consists of eight quadratic function segments in general, four parabolas and four hyperbolas. This is valid in the general case for $d/D \in [0, 1]\backslash\{1/2\}$, i.e. except in the special case for $d/D = 1/2$ where hyperbolas vanish and only four parabolas remain.

Definition 2: Metacentric locus M-curve properties for rectangular cross section

The rectangular cross section has twelve cusp discontinuities of its metacentric locus M-curve in the case where condition $d/D \geq D/(2B)$ ($\lambda \geq 1/(4w)$) is valid, in [5], or $d/D < 1/2 \cdot \tan\beta$, in [4], where β is the angle of the diagonal. For the case where condition $d/D < D/(2B)$ ($\lambda < 1/(4w)$) or $d/D \geq 1/2 \cdot \tan\beta$ is valid, hyperbolic part of the metacentric curve has minimum or maximum on the line $y = \pm x$, and the metacentric locus has sixteen cusps with swallowtail type discontinuities.

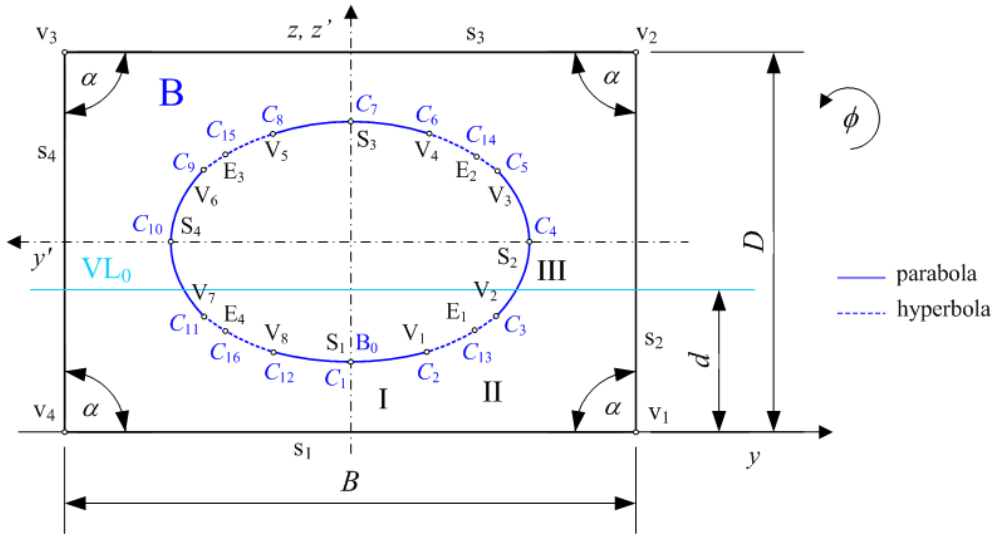

Fig. 1 Rectangular cross shape centre of buoyancy segments with cusp discontinuities

The B-curve quadratic functions segments from the Definition 1 are divided by eight points V, representing geometry vertices intersection points with waterline WL, where rectangular cross section vertices v and its sides s immerse in liquid fluid or emerge from it,

with corresponding deck immersion/bottom emersion of a pontoon. Those V points are eight evolute M-curve cusp discontinuities also, with four more point S coming from semi-cubic parabola cusp discontinuities in their symmetry line, where belonging to B-curve has local extreme. Besides those twelve cusp points C, additional four E points can occur for hyperbola's parts of B-curve when extremes of those curves exist, giving a total of sixteen cusp points C for heel angles ϕ_i, i = 0, …, 15, as mentioned in *Definition 2*, which is all examined in detail in this paper.

In the naval architecture theory, regarding ship stability, the goal is observing the centre of buoyancy B-curve and its evolute M-curve for heel angles ϕ, and therefore, in order to investigate the evolute of the centre of buoyancy B-curve for heel angle ϕ, three ranges, I) to III), are determined for the first coordinate system quadrant, as shown in Fig. 1, using horizontal and vertical symmetry of a rectangular cross section:

Range I): From the first cusp discontinuity C_1 to the second cusp discontinuity C_2, i.e. from the heel angle $\phi_0 = 0°$ or the first parabola symmetry point S_1 to the first vertex intersection point and belonging heel angle $\phi_1 = V_1$,

Range II): From the second cusp discontinuity C_2 to the third cusp discontinuity C_3, i.e. from the first vertex intersection heel angle $\phi_1 = V_1$ to the second vertex intersection heel angle $\phi_2 = V_2$,

Range III): From the third cusp discontinuity C_3 to the fourth cusp discontinuity C_4, i.e. from the second vertex intersection heel angle $\phi_2 = V_2$ to the heel angle $\phi_3 = 90°$ or the second parabola symmetry point S_2.

Accordingly, by *Definition 2*, the metacentric M-curve, as the evolute of the centre of buoyancy B-curve, has twelve cusp discontinuities C, forming butterfly type discontinuity near vertical symmetry line, around heel angles ϕ equal 0 and 180°, for the condition $d/D \geq D/(2B)$, or sixteen where $d/D < D/(2B)$. The conditions for the existence of additional four extreme cusp discontinuities are then set; the first regarding the relation between rectangle particulars draught d, height D and breadth B, and the second regarding the existence of local extreme of metacentric M-curve in hyperbola segment, i.e. heel angle Range II).

Condition 1: The rectangle particulars relation condition for hyperbola extreme existence

$$d/D < D/(2B) \tag{1}$$

Condition 2: The local centre of buoyancy B-curve extreme condition in the hyperbola segment

$$X'_B = 0 \tag{2}$$

where $X_B \equiv \{y_B, z_B\}$ is the centre of buoyancy B-curve.

Since the evolutes of parabola and hyperbola are semi-cubical parabola and Lamé curve with 2/3 exponent and negative sign, they both have cusp discontinuity in the horizontal symmetry at their z–axis, as shown in Fig. 2 and Fig. 3 in the Subchapter 1.2, below. Therefore, belonging metacentric M-curve has eight segments overall. Also, M-curve can have eight symmetry cusp discontinuities, S and E, plus eight vertex intersection cusp discontinuities V, i.e. sixteen cusp discontinuities overall as stated in *Definition 2* above. It is examined in detail in this paper with the emphasis on non-dimensional bounds from *Condition 1*, while the detailed examination of belonging B-curve parabolas and hyperbola equations, together with M-curve equations for semi-cubical parabolas and above mentioned Lamé curve, are given in part two of this paper.

The basics of the centre of buoyancy B-curve and metacentric M-curve equations are given in the introduction with belonging evolute graphs showing their cusp discontinuities in the symmetry of their abscissae definition.

The equations for the determination of vertex cusp discontinuity heel angles ϕ_{V1} and ϕ_{V2} for which rectangular geometry intersects with waterline WL depending on the A/A_T criterion are given in Chapter 2, along with their values. After a detailed examination of the condition for the existence of extreme cusp discontinuity of metacentric M-curve for different non-dimensional breadth to height *B/D* ratios, the new corrected bounds are given in Subchapter 3.3 giving a single necessary existence condition tool for detecting this feature for the rectangular cross section.

The example of an actual rectangular cross section centre of buoyancy B-curve and metacentric M-curve is then given in Chapter 4 for the situation of the existence of sixteen cusps, showing it graphically and explaining this feature of the swallowtail cusp discontinuity existence.

Therefore, in order to investigate the additional cusp discontinuity occurrence for the rectangular cross section, a theoretical re-examination of the centre of buoyancy B-curve and its metacentric locus M-curve is performed in this paper to explain this additional hydrostatic feature.

1.2 General quadratic functions and their evolutes

The metacentric curve characteristics are well studied in the hydrostatic theory of the floating bodies, [21], [22], [23], as well as in the mathematical singularity theory, [5], [4]. This curve basically depends on the centre of buoyancy B-curve characteristics, as it analytically represents the metacentric locus or evolute M-curve of the centre of buoyancy B-curve $z = f(y)$ of a floating body, with the equation:

$$\mathrm{M} = \left(1 + z'^2\right)^{\frac{3}{2}} / z'' \tag{3}$$

In the naval architecture theory, the relation for the determination of the metacentre $\mathrm{M}(y_M, z_M)$ position for the known centre of buoyancy $\mathrm{B}(y_B, z_B)$ and for given heel angle ϕ, can be obtained using actual metacentric radius $r = \overline{\mathrm{MB}} = I/\nabla$ value with

$$y_M = y_B + I(\phi)/\nabla \sin\phi \tag{4}$$

$$z_M = z_B + I(\phi)/\nabla \cos\phi \tag{5}$$

where I is the moment of inertia of waterline WL and ∇ is volume displacement.

Above parametric equations (4) and (5) are further used for metacentric M-curve determination in the paper, while the character of the curves is determined using exact equations from the Table 1 below, obtained using equation (3).

Table 1 Evolutes of the centre of buoyancy curve equations for rectangle and isosceles triangle

Cross section geometry	Metacentric Curve Equation	Description
Rectangle	$y^2 = \frac{8}{27}\left(\frac{z^3}{p} - 3z^2 + 3pz - p^2\right)$	Semi-cubical Parabola $p = b^2/a$
Isosceles Triangle and Isosceles Trapezoid	$(az)^{\frac{2}{3}} - \left(\frac{2b}{3}y\right)^{\frac{2}{3}} = \left(\frac{4b^2}{9} + a^2\right)^{\frac{2}{3}}$	Cuspidal Lamé curve $a = 2/3d$

The centre of buoyancy B-curve evolutes or metacentric M-curves for rectangular and triangular cross shapes are defined in theory explicitly, [1], with equations shown in Table 1, above. For parabola, it is semi-cubical parabola, and for hyperbola it is Lamé curve with exponent 2/3 and minus sign. Since this phrase for Lamé curve is long, it is shorted in some places during the text to the cuspidal Lamé curve, similar to the cuspidal cubic term for semi-cubical parabola sometimes used in theory.

Both of the functions in Table 1 are even functions, horizontally symmetrical, and therefore have cusp discontinuity for even keel or zero heel angle ϕ. While the semi-cubical parabola has the origin of her local coordinate system set to the initial rectangle centre of buoyancy B_0, Lamé curve, as the evolute for triangle and trapezoid shape, has the origin in the keel point K in the centreline C.L. of the pontoon, as shown in Fig. 2 and Fig. 3, below.

Semi-cubical parabola

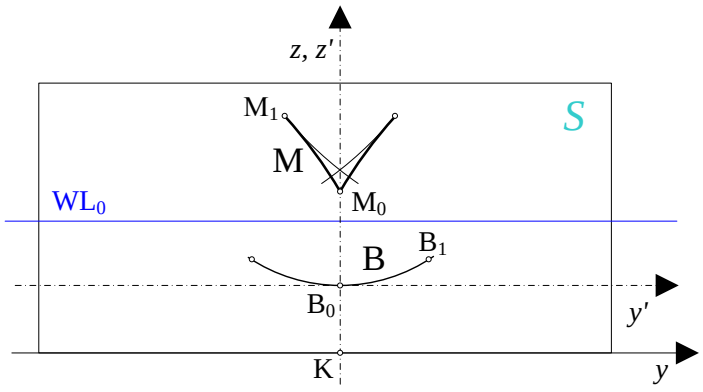

Fig. 2 Symmetric semi-cubical parabola M curve with butterfly type discontinuity

It can be seen from Fig. 2 that the semi-cubical parabola forms butterfly discontinuity type for the parabolic centre of buoyancy B-curve, for rectangular cross section shape of the pontoon at zero heel angle $\phi = 0°$, with two symmetrical branches around the middle cusp discontinuity in initial metacentre point M_0. The end of the left branch is then at a point M_1, where inclined waterline WL intersects the first rectangle deck immersion/bottom emersion point coinciding with one of rectangle vertices v.

Lamé curve with exponent 2/3 and the negative sign

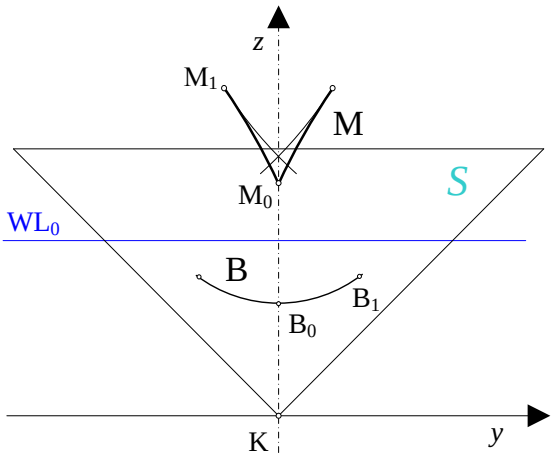

Fig. 3 Symmetric cuspidal Lamé M-curve, with butterfly type discontinuity

Similar to the semi-cubical parabola, it can be seen from Fig. 3 that the cuspidal Lamé curve forms butterfly discontinuity type for the hyperbolic centre of buoyancy B-curve segment obtained for isosceles triangle cross section shape of the pontoon, too. Two symmetrical branches around middle cusp discontinuity in initial metacentre point M_0 of the pontoon, at zero heel angle ϕ.

Therefore, the quadratic functions for the centre of buoyancy B-curve and metacentric M-curve are set here for regular cross section shapes, for heel angles until the first vertex intersection heel angle V_1. But, of course, the metacentre curve continues after it and their analytical functions should be determined where possible to evaluate those values theoretically. Since both quadratic functions, parabola and hyperbola, and belonging metacentric curve segments have cusp discontinuity in their vertical symmetry line, the number of cusp discontinuities for the rectangle can be maximally eight S and E symmetry cusps plus eight vertex intersection points V, as mentioned before in *Definition 2*.

2 Deck immersion/bottom emersion immersion angles

Definition 2 from the introduction of this paper states that the metacentric curve for the rectangular cross section can have eight S and E cusp discontinuities coming from parabola and hyperbola evolute curves cuspidal characteristics, described in the previous Subchapter 1.1, and eight from rectangle vertices intersection with waterline WL, i.e. deck immersion/bottom emersion vertex cusp discontinuities V. In order for one to determine deck immersion/bottom emersion angles for some general convex cross section shapes, it is necessary to find the immersion shape with the basic condition being that obtained volume displacement V equals initial one V_0 for even keel, i.e. there is a condition of constant volume displacement:

$$V = V_0 \tag{3}$$

For a rectangular pontoon of unit length, i.e. for $L = 1$, the cross sectional area of rectangle A must satisfy the initial area A_0 equation condition with

Condition 3: Constant cross section area condition (displacement)

$$A = A_0 \tag{4}$$

By knowing rectangle sides equations $\mathrm{s} \equiv \{z = 0,\ y = -B/2,\ z = D,\ y = B/2\}$, and vertices positions $\mathrm{v} \equiv \{\{-B/2,\ 0\},\ \{-B/2,\ H\},\{B/2,\ 0\},\ \{B/2,\ H\}\}$, belonging rectangle vertices intersection heel angles ϕ_V can be determined from the constant area condition and waterline WL equation as

$$z = y \tan \phi_V + l \tag{5}$$

I.e.:

$$\phi_V = \tan^{-1}\left(\frac{z_2 - z_1}{y_2 - y_1}\right) \tag{6}$$

After that, one of the vertex positions v represents one point $P_1(y_1, z_1)$ in the above equation. Belonging vertices intersection heel angles $\phi_V \equiv \mathrm{V}$ can then be determined by finding the second WL intersection point $P_2(y_2, z_2)$ with general cross section sides which satisfies *Condition 3* in (7).

Depending on the pontoon's immersed area $A = A_0$ to total cross section area A_T ratio A/A_T, the next condition regarding rectangular cross section area can be set:

Condition 4: The condition for the existence of the vertex heel angle

– For A/A_T = 1/2, one intersection heel angle ϕ_V occurs in each coordinate system quadrant, four overall, with two vertices intersection angle coinciding with each other.
– For A/A_T = [0, 1]\{1/2}, two vertices intersection heel angles ϕ_V occur in each coordinate system quadrant, eight overall.

For above heel angles ϕ_V, defined vertices cusp discontinuities V occur. Belonging deck immersion/bottom emersion immersion shapes for a rectangle are then perpendicular triangles or perpendicular trapezoids, as shown in Fig. 4 below.

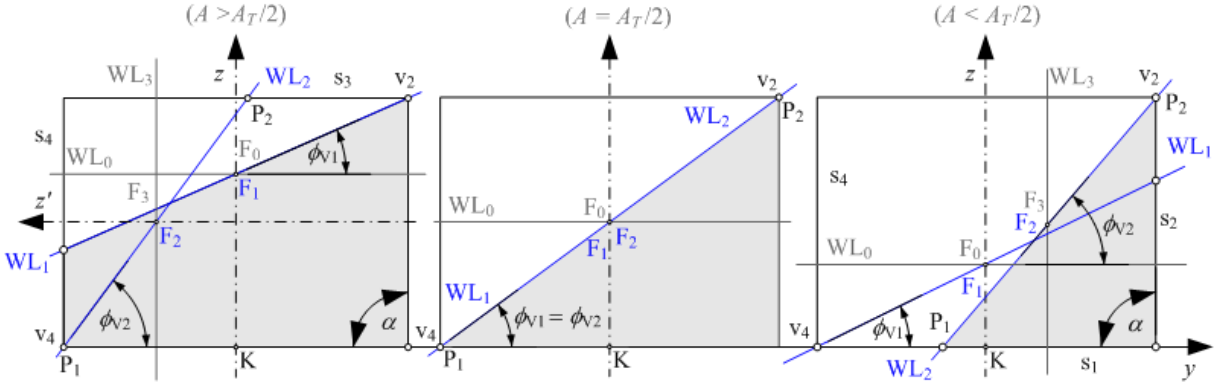

Fig. 4 Deck immersion/bottom emersion immersion shapes for rectangle

2.1.1 Case $A/A_T>1/2$

In the case $A/A_T>1/2$, for the first coordinate system quadrant heel angles ϕ, the resulted immersion shapes are rectangular trapezoids and belonging vertex intersection angles ϕ_V are:

– For the side $s_4 \equiv y_1 = -B/2$, ϕ_{V1}: $A = (D + z_1)\cdot B/2 \rightarrow z_1 = 2A/B - D$

By knowing the vertex $v_2 \equiv \{B/2, D\}$ position, $y_2 = B/2$ and $z_2 = D$, and from (9) it is

$$\phi_{V1} = \tan^{-1}\left(\frac{D - 2A/B + D}{B/2 + B/2}\right) = \tan^{-1}\left(\frac{2(BD - A)}{B^2}\right) \phi_{V1} = \tan^{-1}\left(\frac{2(BD - Bd)}{B^2}\right)$$

$$V_1 \equiv \phi_{V1} = \tan^{-1}\left(\frac{2(D-d)}{B}\right) \tag{7}$$

– For the deck $s_3 \equiv z_2 = D$, ϕ_{V2}: $A=(B/2 + y_2)D/2+(B/2 - y_2)D \rightarrow A = BD/4+y_2D/2+BD/2-y_2D$

$\rightarrow A = 3BD/4 - y_2D/2 \rightarrow A = D/2(3B/2 - y_2) \rightarrow y_2 = 3B/2 - 2A/D$

By knowing the vertex $v_4 \equiv \{-B/2, 0\}$ position, $y_1 = -B/2$ and $z_1 = 0$, from (9) it follows

$$\phi_{V2} = \tan^{-1}\left(\frac{D - 0}{3B/2 - 2A/D + B/2}\right) = \tan^{-1}\left(\frac{D}{2B - 2A/D}\right) = \tan^{-1}\left(\frac{D^2}{2(BD - Bd)}\right)$$

$$V_2 \equiv \phi_{V2} = \tan^{-1}\left(\frac{D^2}{2B(D-d)}\right) \tag{8}$$

2.1.2 Case $A/A_T=1/2$

In the special case where $A/A_T=1/2$, for the first coordinate system quadrant heel angles ϕ, the resulted immersion shapes are rectangular triangles and belonging vertex intersection V_1 and V_2 angles ϕ_V coincide with each other as:

$$V_1 = V_2 \equiv \phi_{V1} = \phi_{V2} = \tan^{-1}\left(\frac{D}{B}\right) \tag{12}$$

2.1.3 Case $A/A_T < 1/2$

For the first coordinate system quadrant heel angles ϕ, and condition $A_0/A_T \leq 1/2$, the resulted immersion shapes are triangles and belonging vertex intersection angles ϕ_V are then:

– For the side $s_2 \equiv y_2 = B/2$, ϕ_{V1}: $A = z_2 \cdot B/2 \rightarrow z_2 = 2A/B$

By knowing the vertex $v_4 \equiv \{-B/2, 0\}$ position, $y_1 = -B/2$ and $z_1 = 0$, from (9) it follows

$$\phi_{V1} = \tan^{-1}\left(\frac{2A/B}{B/2 + B/2}\right) = \tan^{-1}\left(\frac{2A/B}{B}\right) = \tan^{-1}\left(\frac{2A}{B^2}\right) = \tan^{-1}\left(\frac{2Bd}{B^2}\right)$$

$$V_1 \equiv \phi_{V1} = \tan^{-1}\left(\frac{2d}{B}\right) \tag{13}$$

– For the bottom $s_1 \equiv z_1 = 0$, ϕ_{V2}: $A = H(B/2 - y_1)/2 \rightarrow y_1 = B/2 - 2A/D$

By knowing the vertex $v_2 \equiv \{B/2, D\}$ position, $y_2 = B/2$ and $z_2 = D$, from (9) it follows

$$\phi_{V2} = \tan^{-1}\left(\frac{D - 0}{B/2 - B/2 + 2A/D}\right) = \tan^{-1}\left(\frac{D}{2A/D}\right) = \tan^{-1}\left(\frac{D^2}{2A}\right)$$

$$V_2 \equiv \phi_{V2} = \tan^{-1}\left(\frac{D^2}{2Bd}\right) \tag{14}$$

In this way, the heel angles of the vertex cusp discontinuities V_1 and V_2 are determined for the first coordinate system quadrant for all cases depending on the A/A_T condition. The equations (10) to (14) are further used for the determination of Range II) heel angle region and possible occurrence of swallowtail extreme cusp discontinuity for the hyperbola segment of M-curve.

3 Parametric Cartesian "Hydrostatic Particulars Centres Components"

3.1 Parametric form of local extreme cusp discontinuity condition

According to *Definition 2*, the condition for the existence of the swallowtail extreme type cusp discontinuity is set in (2), using the existence of the local extreme of the centre of buoyancy B-curve. For the first coordinate system quadrant, it means that if the local extreme of the centre of buoyancy B-curve function between two vertices heel angles V_1 and V_2 exists, then the extreme type cusp discontinuity of metacentric M-curve exists, too.

This is more suitable in parametric form with

$$y'_M(\phi) = 0 \tag{15}$$

$$z'_M(\phi) = 0 \tag{16}$$

Therefore, the condition for the existence of local extreme Condition 2 can be written as:

Condition 5: The additional condition for the existence of extreme type cusp discontinuity of rectangular cross section metacentric M-curve

If the local extreme heel value of the centre of buoyancy B-curve components exists in between two vertex heel angles, then its metacentric curve has swallowtail extreme cusp discontinuities between two vertex heel angles.

Condition 5 can be used further on to explore the existence of four additional extreme cusp discontinuities E in the hyperbola segments of the B-curve, in total. That is, a single one of them can be found in the Range II) of heel angles using quadratic functions evolutes of the metacentric M-curve, with graphical representation using parametric Cartesian "Hydrostatic Particulars Centres Components" diagram in the next subchapter.

3.2 "Hydrostatic Particulars Centres Components" Diagram

The extreme cusp discontinuities E can be also found graphically using the parametric Cartesian "Hydrostatic Particulars Centres Components" diagram for heel angles ϕ with the distribution of components of hydrostatic centres of buoyancy B-curve, y_B and z_B, waterline F-curve, y_F and z_F, and metacentric M-curve, y_M and z_M, as shown in Fig. 5 below.

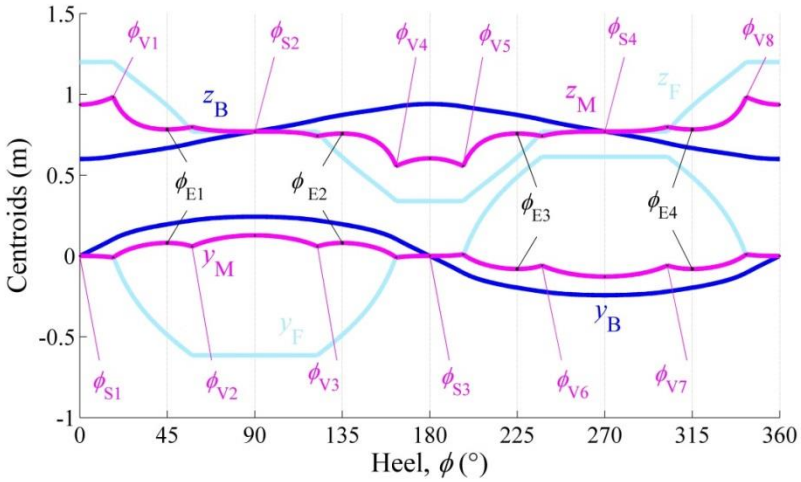

Fig. 5 Hydrostatic particulars centres components for heel angles ϕ for rectangle

It can be seen from the diagram in Fig. 5, and Fig. 1, that there are twelve cusp discontinuity heel angles φ_{Ci}, $i = 0, \ldots, 11$; of metacentric M-curve, designated by small black dot points, with eight of them being vertex discontinuity heel angles ϕ_V, two in every coordinate system quadrant. Four of them are symmetry cusp discontinuity angles ϕ_S with one located in every quadrant of $y - z$ coordinate system, as shown in Fig. 5, with heel angles 90°, 180°, 270° and 360°.

Yet, the "Hydrostatic Particulars Centres Components" diagram in Fig. 5 shows the situation where additional extreme cusp discontinuities of the extreme metacentric curve discontinuity type occur when metacentric curve components have an extreme value between two vertex heel angle values of the rectangle side. In other words, those are cusp discontinuities that occur for extreme heel angles ϕ_{Ej}, $j = 1, \ldots, 4$, between vertex cuspidal heel angles ϕ_V, with one of them in every quadrant of the coordinate system. Namely, there are four of them, all together, with values $\phi_E = \{45°, 135°, 225°, 315°\}$, giving additional four cusp discontinuities $\varphi_{Ci,}$ $i = 12, \ldots, 15$. Thus, it shows the existence of additional extreme cusp discontinuities that are expected for this rectangle draught according to *Condition* 2 and *Condition* 5.

Therefore, cusp discontinuity heel angles ϕ_C can be divided into two types:

1. Extreme type, E, where metacentric locus M-curve components, y_M and z_M, have local extremes, for heel angles of rectangle symmetry: ϕ_0, ϕ_3, ϕ_6, ϕ_9, i.e. angles $\phi_S = \{0°, 90°, 180°, 270°, 360°\} \in \phi_C$; and hyperbola extreme angles $\phi_E = \{45°, 135°, 225°, 315°\}$.

2. Vertex type, V, where metacentric locus M-curve components, y_M and z_M, have cusp discontinuities, too, with two of them in every coordinate system quadrant, for heel angles of waterline intersection WL with rectangle vertices V: ϕ_1 and ϕ_2, ϕ_4 and ϕ_5, ϕ_7 and ϕ_8, and ϕ_{10} and ϕ_{11}, i.e. angles ϕ_V = {17.176°, 57.756°, 122.244°, 162.824°, 197.176°, 237.756°, 302.244°, 342.284°} ∈ ϕ_C.

So, it can be concluded that cusp discontinuity occurs for the either local extreme of metacentric locus M-curve components or vertex heel angles V of pontoon sides s emersion/immersion. Additionally, since these angles occur for $\phi_E = 45° + k \cdot 90$, k = 0, …, 3 angles, the extremes of hyperbola occur on $y' = \pm x'$ lines, as defined in *Definition* 2 at the beginning of the paper, and therefore it is confirmed.

3.3 The rectangle particulars ratios condition for the existence of extreme cusp discontinuity

The existence of extreme cusp discontinuity in the Range II of heel angles is examined here with the examples of hydrostatic particulars curves calculated for several draughts of rectangular cross section pontoons with unit length L = 1(m), in order to examine the influence of rectangular cross section pontoon B/D ratio on additional cusp discontinuity occurrence. The first one is from this paper calculation example with particulars: Breadth B = 2.2 (m) and Height D = 1.54 (m), or B/D = 2.2/1.54. After that, additional calculations are performed for pontoons with B/D = {0.5, 0.75, 1, 2, 3} with constant height D = 1.54 (m). The chosen draughts are d = {0.3, 0.6, 0.77, 1.0, 1.1, 1.2, 1.4} (m), and the example from this paper of d = 1.2 (m) and from the Uršić textbook, [23], of d = 1.1 (m) are used for comparison. The results are given in Table 2, with red colour showing the cases where *Condition 1* with $d/D < D/(2B)$ is satisfied, and a column showing the existence/absence of swallowtail cusp discontinuity with extreme cuspidal heel angle ϕ_{E1} = 45°.

Table 2 The existence of additional cusp discontinuity for rectangular cross sections

		d (m)	0.3	0.6	0.77	0.9	1	1.1	1.2	1.4
B/D	$D/(2B)$	d/D	0.1948	0.3896	0.5	0.5844	0.6494	0.7143	0.7792	0.9091
0.5	1	Cusp	Yes	No	No	No	No	No	Yes	Yes
		ϕ_1 (°)	37.926	57.313	63.435	58.97	54.513	48.184	41.448	10.135
		ϕ_2 (°)	78.977	68.714	63.435	59.697	57.002	54.462	52.074	79.695
0.75	0.6̇	Cusp	Yes	No	No	No	Yes	Yes	Yes	Yes
		ϕ_1 (°)	27.451	46.095	53.13	47.939	43.078	37.304	30.487	13.627
		ϕ_2 (°)	73.711	59.697	53.13	58.062	62.257	66.801	71.677	82.235
1.0	0.5	Cusp	Yes	Yes	No	Yes	Yes	Yes	Yes	Yes
		ϕ_1 (°)	21.286	37.926	45	39.732	35.042	29.745	23.824	10.305
		ϕ_2 (°)	68.714	52.074	45	50.268	54.958	60.255	66.176	79.695
2.2/1.54	1.54/4.4	Cusp	Yes	No	No	No	No	Yes	Yes	Yes
		ϕ_1 (°)	15.255	28.61	34.992	30.192	26.147	21.801	17.176	7.253
		ϕ_2 (°)	60.9	41.934	34.992	40.104	44.947	50.774	57.756	75.44
2.0	0.25	Cusp	Yes	No	No	No	No	No	Yes	Yes
		ϕ_1 (°)	11.023	21.286	26.565	22.567	19.323	15.945	12.45	5.194
		ϕ_2 (°)	52.074	32.687	26.565	31.03	35.487	41.186	48.552	70.017
3.0	0.16̇	Cusp	No	No	No	No	No	No	No	Yes
		ϕ_1 (°)	7.4	14.56	18.435	15.486	13.158	10.784	8.373	3.468
		ϕ_2 (°)	40.549	23.16	18.435	21.853	25.422	30.256	37.049	61.39

It can be seen from Table 2 that the extreme cuspidal heel angles E in the first quadrant exist if the first vertex heel angle ϕ_1 is lower than 45° and the second vertex heel angle ϕ_2 is larger than 45°. Therefore, *Condition 1* is not correct and should be replaced with a new condition for the existence of additional cusp discontinuity for the rectangular cross section in the first quadrant with:

Condition 6: *The single necessary condition for the existence of extreme cusp discontinuity in the hyperbola segment of heel angles for rectangular cross section*

In order for extreme cusp discontinuity to exist in hyperbola segment of heel angles, the first vertex cuspidal heel angle must be lower than 45° and the second vertex cuspidal heel angle must be higher than 45°.

Mathematically written, the necessary condition for the existence of extreme cusp discontinuity and its heel angle in the first coordinate system quadrant is:

$$\phi_{E1}: \phi_1 \leq 45° \;\&\; \phi_2 \geq 45° \tag{17}$$

If the existence *Condition 6* in the equation (17) is satisfied, then the rectangular cross section pontoon has extreme cusp discontinuity heel angle φ_{E1} at 45° for actual loading condition with draught d, confirming *Definition 2* of this paper, and it is on a line in a local coordinate system $y' = \pm x'$ with origin in the rectangle's v_1 vertex.

Another meaning of *Condition 6* is that there are lower and upper bounds for the existence of extreme cusp discontinuity in the hyperbola segment of heel angles, i.e. swallowtail discontinuity, and they are determined below.

The limit draught ranges for B/D ratios can be then determined using basic equations (10) to (14), from Chapter 2, for the calculation of vertex heel angles ϕ_{V1} and ϕ_{V2}, that depend on d/D i.e. A/A_T value. Namely, there are two cases and they are: 1. $d/D \leq 1/2$ ($A/A_T \leq 1/2$) and 2. $d/D > 1/2$ ($A/A_T > 1/2$), with the first producing triangular and the second producing quadrilateral immersion shapes, as shown in Fig. 4. The results of the calculation are shown in Table 3 below, with steps for non-dimensional B/D and d/D ratios determination, and B/D ratio being chosen due to naval architecture practice in ship theory where this ratio is common non-dimensional variable.

Table 3 Determination of additional cusp discontinuity occurrence limit curves

Steps	**$d/D \leq 1/2$ ($A/A_T \leq 1/2$)**	**$d/D > 1/2$ ($A/A_T > 1/2$)**
1	$\tan\varphi_1 = 2d/B$	$\tan\varphi_1 = 2(D-d)/B$
	$\tan\varphi_2 = D^2/(2Bd)$	$\tan\varphi_2 = D^2/[2B(D-d)]$
2	$\tan\varphi_1 = 2d/B = 2d/D \cdot D/B = 2y/x$	$\tan\varphi_1 = 2\ D/B(1-d/D) = 2(1-y)/x$
	$\tan\varphi_2 = D^2/(2Bd) = 1/2D/d \cdot D/B$ $\tan\varphi_2 = 1/(2xy)$	$\tan\varphi_2 = D^2/[2B(D-d)] = 1/[2B/D(1-d/D)]$ $\tan\varphi_2 = 1/[2x(1-y)]$
3	$1 = 2y/x \rightarrow y = x/2$	$1 = 2(1-y)/x \rightarrow y = 1 - x/2$
	$1 = 1/(2xy) \rightarrow y = 1/(2x)$	$1 = 1/[2x(1-y)] \rightarrow y = 1 - 1/(2x)$

The equations for vertex heel angles V are determined first, in step 1; then non-dimensional B/D and ratios d/D are introduced in step 2, and finally $x = B/D$ and $y = d/D$ are replaced by x and y, respectively, while $\tan\phi_1$ and $\tan\phi_{2\ are}$ set to $\tan(45°) = 1$ according to equations (10) to (14), in step 3.

Therefore we get two straight lines and two rectangular hyperbolas, as lower $(d/D)_L$ and upper limits $(d/D)_U$. The lower limits $(d/D)_L$ are: $y = x/2$ for $B/D < 1$ and $y = 1/(2x)$ for $B/D > 1$, while upper limits $(d/D)_U$ are: $y = 1 - x/2$ for $B/D < 1$ and $y = 1 - 1/(2x)$ for $B/D > 1$.

After drawing the above limit curves, the areas with and without additional extreme cusp discontinuity are shown in Fig. 6 below.

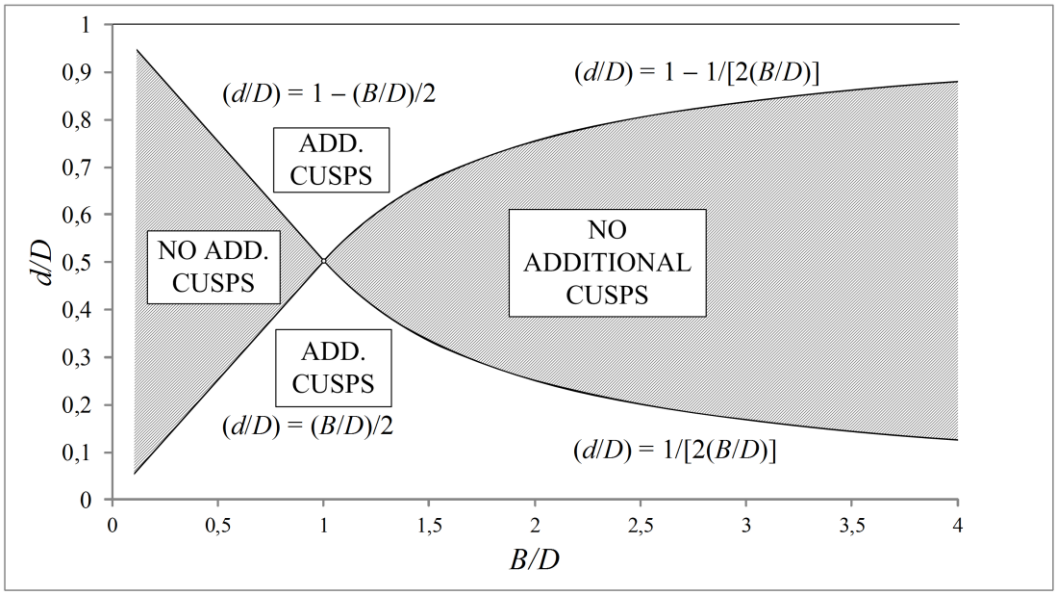

Fig. 6 Additional extreme cusp discontinuity areas for B/D and d/D values

Above diagram shows areas where additional extreme cusp discontinuity occurs for hyperbola segment heel angle region Range II). If an additional cusp exists, the swallowtail discontinuity exists and the metacentric M-curve has sixteen cusp discontinuities overall, thus proving *Definition 2*. It should be noted that the point $\{d/D = 0.5, B/D = 1\}$ also belongs to the additional extreme cusp discontinuity according to *Condition 6*, i.e. the swallowtail discontinuity always exists for $B/D = 1$, as shown in Fig. 6 above.

Condition 6 differs from *Condition 1* from *Definition 2* set in the theory before and represents a single necessary condition for the existence of the extreme cusp discontinuity for rectangular cross sections.

4 Example - metacentric curve cusp discontinuities in hyperbola segment

In this chapter, the hydrostatic curves are calculated for the example of a rectangular cross section test pontoon with breadth $B = 2.2$ (m), height $D = 1.54$ (m), length $L = 1$ (m), for draughts $d = 0.3$ (m) with volume displacement $\nabla = 0.66$ (m^3) and draught $d = 1.2$ (m) with volume displacement $\nabla = 2.64$ (m^3) in order to show the range of swallowtail discontinuity existence. Similar calculations are done for different densities of icebergs in [24], but without bounds determination. The hydrostatic properties values for the above examples are rechecked using Ban's polynomial radial basis functions, PRBF, [25], and then graphically represented with Biles like drawings, [26]. The curves shown are the centre of buoyancy B-curve, with components $X_B \equiv \{y_B, z_B\}$ and discrete points B, the centre of waterline F-curve,

with components $X_F \equiv \{y_F, z_F\}$ and discrete points F, and the metacentric M-curve, with components $X_M \equiv \{y_M, z_M\}$ and discrete points M.

4.1 Swallowtail discontinuity between deck immersion/bottom emersion angles

In this subchapter, the hydrostatic curves are calculated for the draughts d = 1.2 (m), with the corresponding centre of buoyancy B-curve and metacentric M-curve, shown in 7 and 8, below.

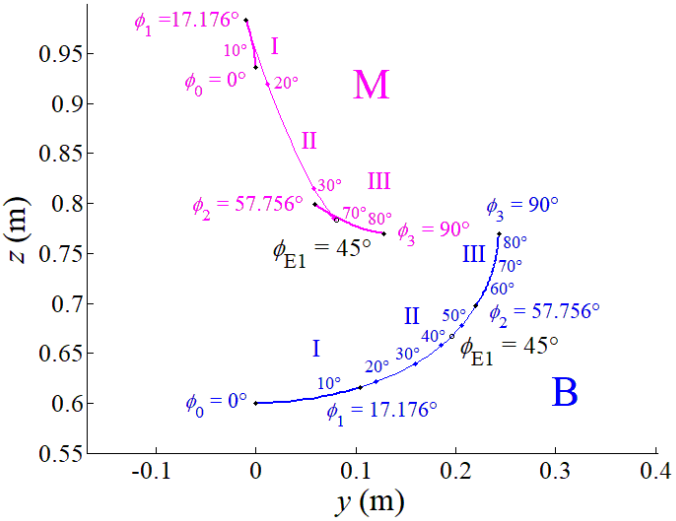

Fig. 7 Metacentric M-curve for rectangular cross section in the first quadrant

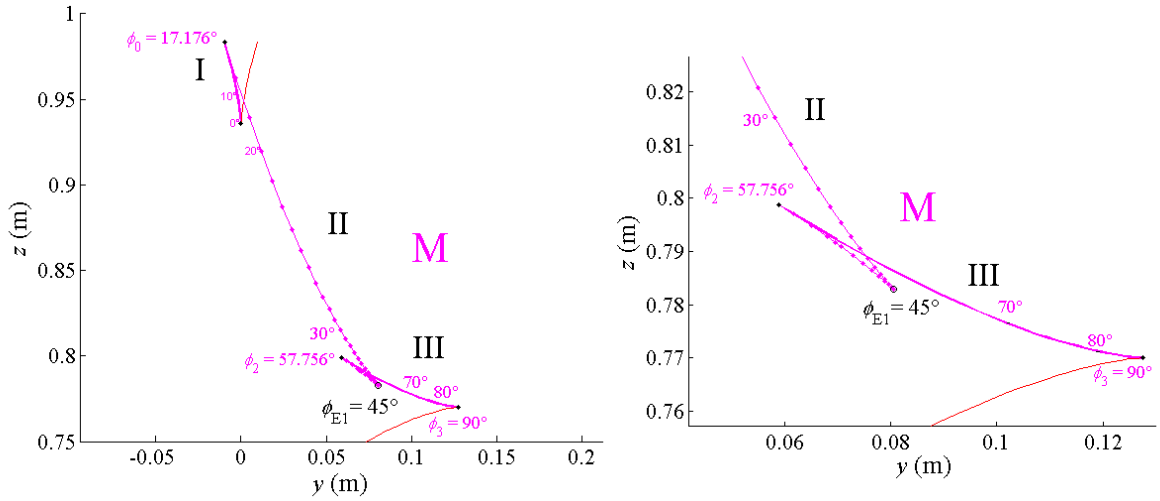

Fig. 8 Metacentric M-curve with zoom of extreme cusp discontinuity for hyperbola

As can be seen in Fig. 7 and Fig. 8, above, the metacentric M-curve has four "regular" cusp discontinuities in the first quadrant, designated by black points and cusp angles ϕ_0 to ϕ_3, with three curve ranges. Yet, Fig. 7 and Fig. 8 show the existence of extreme cusp discontinuity E_1, too, for heel angle $\phi = 45°$, forming swallowtail discontinuity for hyperbola region of heel angles in Range II), as defined in *Definition 2*.

Since extreme cusp discontinuity exists for heel angle $\phi = 45°$, it lays on the line $y' = -x'$ of the local coordinate system set to rectangle vertex point v_1, and therefore partially proves *Definition 2*. But the correct statement for *Definition 2* should be that above extreme cusp discontinuities for rectangle occur for 45° heel angles in every coordinate system quadrant,

i.e. in the middle of the arbitrary shape vertex angle v in general due to B-curve hyperbola segment evolute M-curve characteristics of cuspidal Lamé curve.

4.2 Overall characteristics for whole 360°

In order to show all features of the metacentric M-curve in total, the centres of hydrostatic properties for the test rectangular pontoon are calculated numerically with higher resolution from 0° to 360°, with heel angles distribution of 1°, for draughts d = 0.3 (m) and d = 1.2 (m), i.e. cases $A/A_T < 1/2$ and $A/A_T > 1/2$, respectively.

4.2.1 Case $A/A_T > 1/2$

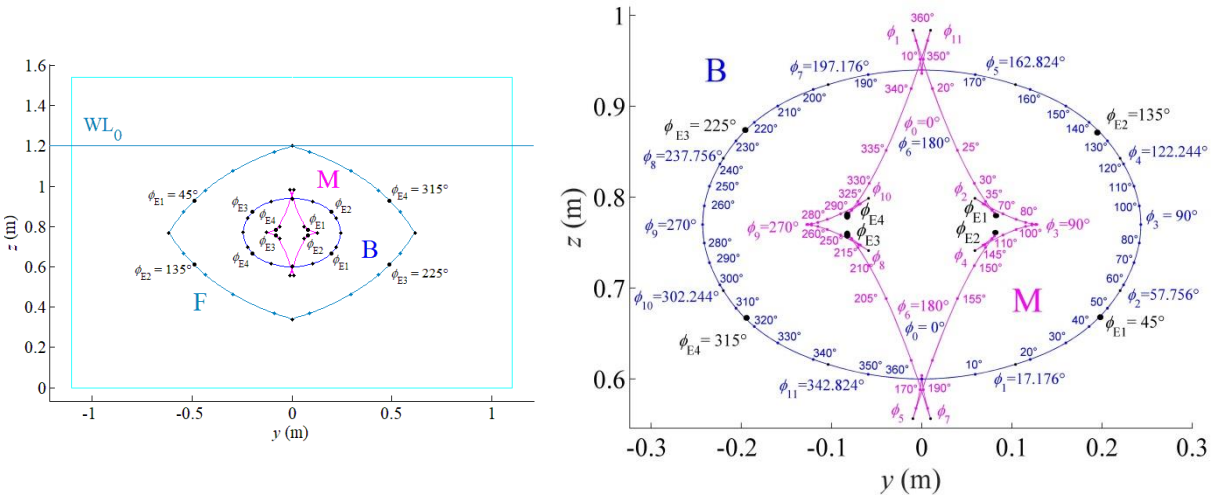

Fig. 9 Hydrostatic properties for rectangular cross section pontoon, case $A/A_T > 1/2$

It is obvious from the "Hydrostatic Particulars Centres" diagrams in Fig. 9, that there are twelve heel angles ϕ_C, c = 0, ... m = 11, with values ϕ_C = {0°, 17.176°, 57.756°, 90°, 122.244°, 162.824°, 180°, 197.176°, 237.756°, 270°, 302.244°, 342.824°, 360°}, for which cusp discontinuities occur on metacentric M-curve for rectangular cross section pontoon. Among them, there are eight vertex heel angles φ_V, v = 1, ... n = 8, with values φ_V = {17.176°, 57.756°, 122.244°, 162.824°, 197.176°, 237.756°, 302.244°, 342.824°}, that dictate the areal characteristics of pontoon centre of waterline F-curve in a known way, where the centre of waterline curve is smooth between two vertex heel angles ϕ_1 and ϕ_2 for some quadrant and stands in a point for other angles. Apart from that, they influence corresponding moment of inertia of the waterline WL area, thus directly dictating the characteristics of the metacentric M-curve, too. Corresponding extreme cuspidal heel angles can be then found in the part of the centre of the waterline curve between vertex heel angle values V_1 and V_2, also, with all four extreme cuspidal heel angles ϕ_{Ei}, i = 1, …, 4, with values ϕ_E = {45°, 135°, 225°, 315°}.

Fig. 9, with Fig. 7 and Fig. 8, show that another metacentric curve cusp discontinuity exists in the range between the first and the second vertex heel angles in all coordinate system quadrants, from ϕ_{E1} to ϕ_{E4}.

And thus, *Definition 2* of this paper is proven graphically.

4.2.2 Case $A/A_T < 1/2$

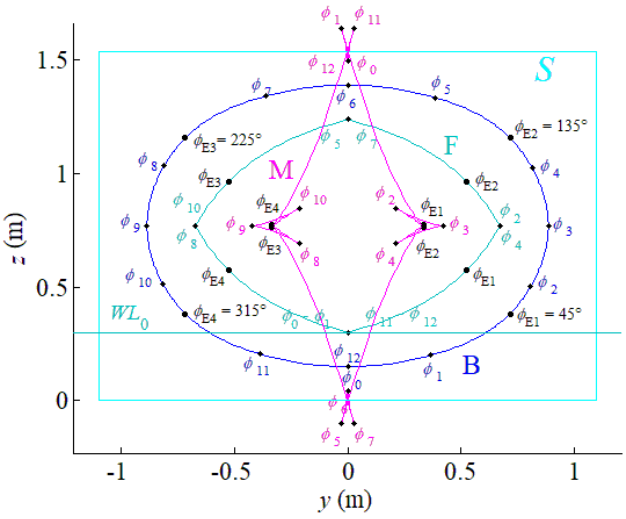

Fig. 10 Hydrostatic properties for rectangular cross section pontoon, case $A/A_T < 1/2$

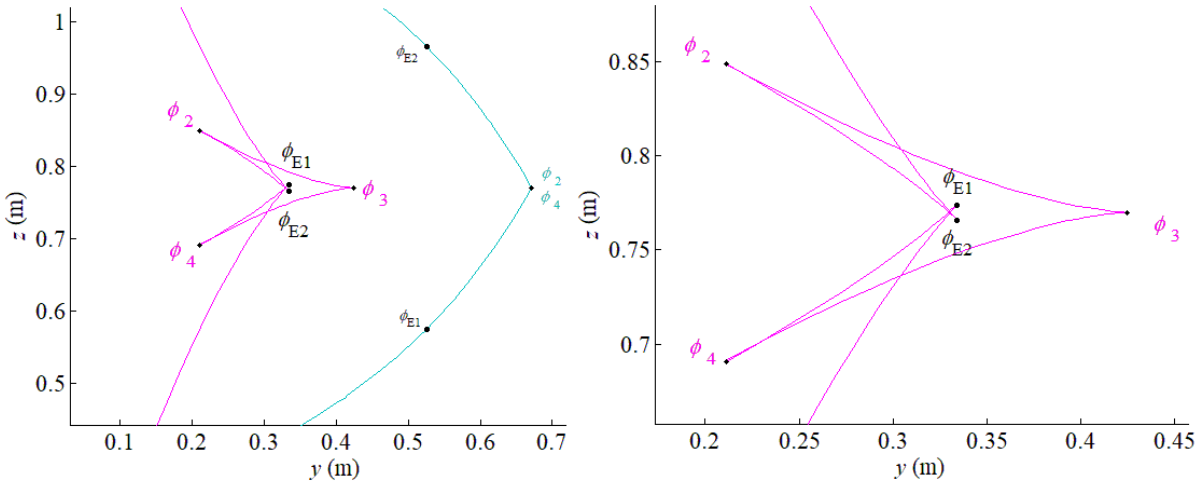

Fig. 11 Zoom of swallowtail discontinuities for rectangular pontoon, case $A/A_T < 1/2$

Fig. 10 and Fig. 11 above, show two overlapping swallowtail discontinuities near ϕ_{E1} and ϕ_{E2} extreme discontinuities, for case $A/A_T < 1/2$, proving their existence below the condition $d/D \geq D/(2B)$ from Definition 2.

Therefore, this represents yet another proof of the need for correction of above mentioned bound in *Condition 1* and the need for setting the bounds from *Condition 6*.

4.3 Examples of real floating objects

Several real floating objects are examined here theoretically for possible additional cusp discontinuity existence: near rectangle cross section pontoons, oil and chemical tankers with high block coefficients, large bulk carriers, general cargo ships and coastal oil tankers.

The results in Table 4, below, show that some real floating objects should be checked for the existence of additional extreme cusp discontinuities since their corresponding hull forms slightly differ from the theoretically rectangular cross section. Among them, ships with higher block coefficients should be specially examined for flat deck cambers that can cause swallowtail cusp discontinuity heel angles of ship immersion, and thus influence the possibility of additional cusp discontinuity occurrence.

Table 4 Examples of additional cusp discontinuities for real objects

	L_{OA} (m)	L_{PP} (m)	B (m)	D (m)	d (m)	B/D	d/D	$(d/D)_U$	Cusp
Pontoon	120.0	-	32.2	8.1	6.2	3.975	0.765	0.874	No
Chemical Oil tanker	182.4	174.8	32.2	18.0	12.18	1.789	0.677	0.720	No
Crude Oil Tanker	380.0	366.0	68.0	35.0	24.5	1.943	0.7	0.743	No
Bulk Carrier	255.0	251.5	32.2	20	14.43	1.610	0.722	0.689	Yes
General Cargo	118.19	115.31	13.35	9.1	6.1	1.467	0.67	0.659	Yes
Coastal Oil Tanker	96	90.2	15.5	7	5.72	2.214	0.817	0.774	Yes

It can be seen from Table 4, above, that some ships should be calculated for denser heel angle ϕ values than usually distributed for 5 or 10°, in order to detect swallowtail type discontinuity. The objects with low B/D ratios near value one should also be specially examined since their whole range of d/D values can result in swallowtail cusp discontinuity occurrence. This will be further studied, as well, by the author in other papers.

4.4 Transversal static stability particulars

After the transversal metacentric curve is known, it is possible to calculate the ship's stability particulars directly, and evaluate the influence of additional metacentric curve cusp discontinuity on stability particulars, as well as on other ship characteristics.

But first, it is necessary to calculate the metacentric height curve for one centre of gravity G position, with components $X_G \equiv \{y_G, z_G\}$. Corresponding actual metacentric height curve c represents the distance from the actual metacentre, M, to the centre of gravity, G, of the ship, for different heel angles ϕ. Corresponding transversal intact stability particulars are calculated for zero transversal centre of gravity, $y_G = 0$ (m), and the vertical centre of gravity of the pontoon is set to $z_G = 0.77$ (m), as shown in Fig. 12 below.

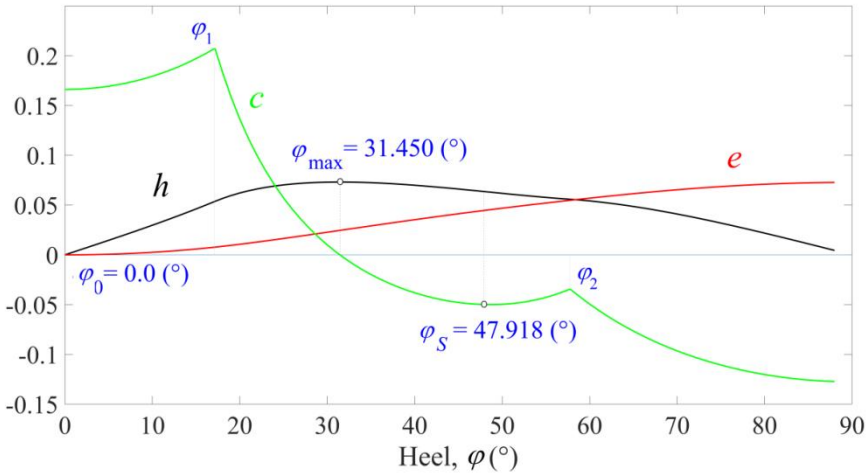

Fig. 12 Elementary transversal stability functions for draught $d = 1.2$ (m)

The results shown in Fig. 12 represent elementary stability functions: metacentric height curve c, transversal static stability righting lever curve h and transversal dynamic stability path curve e.

It is well known that elementary stability functions *c*, *h* and *e* are all interconnected by integration and derivation relations. Therefore, if one curve is known, it is possible to determine all others. One of their possible relations are

$$h = \int_{\varphi} c d\varphi \tag{18}$$

$$e = \int_{\varphi} h d\varphi = \int_{\varphi}\int_{\varphi} c d\varphi d\varphi \tag{19}$$

Obviously, metacentric height curve *c* has the same position of local extremes for vertex heel angles ϕ_{V1} and ϕ_{V2}, as shown in Fig. 12, but a different position of local extreme than metacentric M-curve for extreme cuspidal heel angle ϕ_E. Therefore, it should be calculated separately, by finding a local minimum of metacentric height *c* curve, using the same condition as for additional cusp discontinuity of metacentric M-curve.

The heel angle value for which the metacentric height curve, *c*, has a local minimum angle in the above example is ϕ_S = 47.918(°), which clearly differs from extreme cuspidal heel angle ϕ_E = 45(°), and should be determined separately. For this angle, ϕ_S, the static stability righting lever curve *h* also has a local inflection point, as shown in Fig. 12, and this is an expected feature determined by Zeeman, [4], also. The righting lever curve inflection heel angle value φ_S differs for the different centres of gravity $X_G \equiv \{y_G, z_G\}$ and should be calculated for the actual X_G value.

It can be concluded overall that if the swallowtail type discontinuity exists for some general cross section the intact stability calculations should be performed with denser heel angles ϕ distribution, in order to detect this feature for righting lever curve. The conclusion about the qualitative effect of the swallowtail discontinuity cannot be given solely from this paper, but it can be seen from Fig. 12 that righting lever curve has a larger range and area under it, due to the existence of the inflection point in between of two vertex heel angles of deck immersion/bottom emersion.

5 Conclusion

As the first part of this paper, the centre of the buoyancy curve and metacentric curve of the rectangular cross section shape is re-examined, with correct upper and lower non-dimensional bounds for swallowtail discontinuity existence given, thus enabling easy determination of the above metacentric curve feature. When those conditions are satisfied, additional cusp discontinuities of the metacentric curve for rectangular cross section floating body exists for heel angles equal to 45 degrees, i.e. in the symmetry of the rectangle vertex angles. Then, using the hydrostatic particulars centres components diagram, it is shown that cusp discontinuities for rectangle can be divided into extreme and vertex type discontinuities, with extreme one giving inflection of static stability righting lever curve when swallowtail type discontinuity exists in the hyperbola segment of the centre of buoyancy curve. Overall, the swallowtail discontinuity may be considered positive regarding stability particulars values of wall-sided ships, enlarging range and the area below righting lever curve, which should be further examined.

In part 2 of this paper, the exact centre of buoyancy and metacentric locus curves for the whole first quadrant heel angles will be examined also using quadratic functions.

Since, the above is examined for the regular rectangular shape of a floating body, in the future author's work other regular shapes will be investigated, as well as for the cross-sectional shapes of actual ship hull forms.

Finally, after all the centre of buoyancy and metacentric curves are known, the rectangle's hydrostatic kinematics can be re-examined in detail which will be the future research topic of the author of this paper.

References

[1] Bouguer, P., 1746. Traité du Navire.

[2] Euler, L., 1749. Scientia Navalis.

[3] Thom, R., 1989. Structural Stability and Morphogenesis: An Outline of a General Theory of Models. Reading, MA: *Addison-Wesley* (French edition, 1972).

[4] Zeeman, E. C., 1976. A Catastrophe Model for Stability of Ships. *Geometry and Topology: III Latin American School of Mathematics*, I.M.P.A., Rio de Janeiro, Brazil, 775-827.

[5] Poston, T., Stewart, I., 1978. Catastrophe Theory and its Applications. *Dover Publ. Inc.*, Mineola, New York, USA.

[6] Arnold, V. I., 1992. Catastrophe Theory, *Springer-Verlag*, 3rd ed., Berlin, Germany.

[7] Senjanović, I., Fan, Y., 1994. Dynamic analysis of ship capsizing in regular waves. *Brodogradnja*, 42, 1, 51-60.

[8] Senjanović, I., Fan, Y., 1995. Numerical simulation of ship capsizing in irregular waves. *Chaos, Solitons and Fractals*, 5; 727-737.

[9] Neves, M.A.S., Belenky, V. L., de Kat, J. O., Spyrou, K., Umeda, N., 2011. Contemporary Ideas on Ship Stability and Capsizing in Waves. *Springer*.

[10] Neves, M.A.S., Rodríguez, C.A., 2005. A Non-Linear Mathematical Model of Higher Order for Strong Parametric Resonance of the Roll Motion of Ships in Waves. *Marine Systems & Ocean Technology*, 1(2), 69–81. https://doi.org/10.1007/BF03449197

[11] Makai, A., Miino, Y., Umeda, N., Sakai, M., Ueta, T., Kawakami, H., 2021. Nonlinear dynamics of ship capsizing at sea. *Nonlinear Theory and Its Applications*, *IEICE*, 13(1), 2-24. https://doi.org/10.1587/nolta.13.2

[12] Zhang, Y., Wang, P., Liu, Y., Hu, J., 2021. Nonlinear Rolling Stability and Chaos Research of Trimaran Vessel with Variable Lay-outs in Regular and Irregular Waves under Wind Load. *Brodogradnja*, 72(3), 97-123. https://doi.org/10.21278/brod72307

[13] Spyrou, K. J., 2022. The stability of floating regular solids. *Ocean Engineering*, 257, 111615. https://doi.org/10.1016/j.oceaneng.2022.111615

[14] Nowacki, H., Ferreiro, L. D., 2003. Historical Roots of the Theory of Hydrostatic Stability of Ships. *8th International Conference on the Stability of Ships and Ocean Vehicles*, STAB 2003, 15-19 September, Madrid, Spain, 1-30.

[15] Francescutto, A., Papanikolau, A. D., 2010. Floatability and Stability of Ships: 23 Centuries after Archimedes. *The Genius of Archimedes-23 Centuries of Influence on Mathematics, Science and Engineering*, 8-10 June, Syracuse, Italy, 277-288.

[16] Francescutto, A. 2016. Intact stability criteria of ships – Past, present and future. *Ocean Engineering*, 120, 312-317. https://doi.org/10.1016/j.oceaneng.2016.02.030

[17] Megel, J., Kliava, J., 2010. Metacenter and ship stability. *American Journal of Physics*, 78(7), 738-747. https://doi.org/10.1119/1.3285975

[18] Hantoro, R., Septyaningrum, E., Hudaya, J. R., Utama, I.K.A.P., 2022. Stability Analysis for Trimaran Pontoon Array in Wave Energy Converter-Pendulum System (WEC-PS), *Brodogradnja*, 73(3), 59-68. https://doi.org/10.21278/brod73304

[19] Karolius, K. B., Vassalos, D., 2018. Second generation calculation method for use in the inclining experiment. *Proceedings of 13th International Conference on the Stability of Ships and Ocean Vehicles*, 16-21 September, Kobe, Japan, 421-428.

[20] Santos, T.A., Guedes Soares, C., 2019. Deterministic and probabilistic methods applied to damage stability. *Marine Technology and Engineering*, 1297-1312.

[21] Von den Steinen, C., 1934. Berechnungsunterlagen für Stabilitätsuntersuchungen in der Praxis. *Jahrbuch der Schiffbautechnischen Gesellschaft*, Band 35.

[22] Robb, A. M. 1952. Theory of Naval Architecture. *Griffin*, London, UK.

[23] Uršić, I., 1991. Stabilitet broda I. FSB, *Sveučilišna naklada*, Zagreb.

[24] Nye, J. F., Potter, J. R., 2017. The use of Catastrophe Theory to Analyse Stability and Toppling of Icebergs. *Annals of Glaciology*, 1, 49-54. https://doi.org/10.3189/S0260305500016955

[25] Ban, D., Bašić, J. 2015. Analytical Solution of Basic Ship Hydrostatic Integrals using Polynomial Radial Basis Functions, *Brodogradnja*, 66(3), 15-37.

[26] Biles, J. H., 1908. The Design and Construction of Ships, Vol II: Stability, Resistance, Propulsion and Oscillations of Ships, Historische Schiffarht, Band 92, Salwasser Werlag.

Submitted: 13.12.2022.
Accepted: 08.02.2023.

Dario Ban Dario.Ban@fesb.hr
University of Split
Faculty of Electrical Engineering, Mechanical Engineering and Naval Architecture, 21000 Split; Croatia